LASER & PHOTONICS REVIEWS

www.lpr-journal.org

Room Temperature Synthesis of Stable Zirconia-Coated $CsPbBr_3$ Nanocrystals for White Light-Emitting Diodes and Visible Light Communication

*Qionghua Mo, Chen Chen, Wensi Cai, Shuangyi Zhao, Dongdong Yan, and Zhigang Zang**

The photoluminescence quantum yield (PLQY) of $CsPbBr_3$ perovskite nanocrystals (NCs) prepared by the hot-injection method can exceed 90%, which have attracted intensive attention for white light-emitting diodes (WLEDs). However, the whole hot-injection experiment requires air isolation and relatively high temperature. In addition, the poor stability of $CsPbBr_3$ NCs impedes their applications. Here, a facile method is reported to synthesize $CsPbBr_3$@ZrO_2 NCs at room temperature in air. Owing to using ZrO_2 coated $CsPbBr_3$ NCs, the prepared $CsPbBr_3$@ZrO_2 NCs not only present a PLQY of 80% but also exhibit an enhanced stability to heat and moisture. Furthermore, WLEDs are fabricated with $CsPbBr_3$@ZrO_2 NCs and commercial red phosphors ($CaAlSiN_3:Eu^{2+}$) on blue LEDs chips. The fabricated WLEDs exhibit a correlated color temperature (CCT) of 4743 K and luminous efficacy as high as 64.0 Lm W^{-1}. In addition, visible light communication with a high data rate of 33.5 Mbps is achieved using the WLEDs. This work provides a room temperature strategy to coat zirconia for $CsPbBr_3$@ZrO_2 NCs, benefiting to enhance the optical performance and stability, as well as the promotion of the great potentials in solid-state illuminating and visible light communication applications.

1. Introduction

Nowadays, white light-emitting diodes (WLEDs) have received broad attention and gradually replaced the conventional bulbs and fluorescent lighting sources due to their high luminous efficiency, low driving voltage, energy-saving and long operating lifetime.[1,2] Although commercial WLEDs can be fabricated using InGaN blue chips and yellow-emitting phosphors ($YAG:Ce^{3+}$), it is still quite challenging to develop high efficient luminance WLEDs owing to the lack of green component in the white emission. Therefore, it is necessary to develop high-efficiency luminance materials for WLEDs.

Recently, all-inorganic $CsPbX_3$ (X = Cl, Br, I) nanocrystals (NCs) have attracted broad attention as promising candidates in light-emitting diodes (LEDs),[3–8] solar cells,[9–11] lasers,[12–14] and photodetectors,[15–17] owing to their excellent optoelectronic properties, including high photoluminescence quantum yield (PLQY), wide tunable emission and narrow emission spectrum.[18–20] The relatively higher stability renders $CsPbBr_3$ NCs wide research, but the reported ones still suffer from poor heat and moisture stability, limiting their practical applications.[21–25] Therefore, it is quite urgent to synthesize $CsPbBr_3$ NCs with high stability while maintaining their advantages including high PLQY and narrowband emission. Up to now, various methods have been adopted to improve the optical performance and stability of $CsPbBr_3$ NCs, such as coating, ligand modification, and elemental doping.[26–31] Our group reported a ligand modification by using 2-hexyldecanoic acid (DA) to replace oleic acid (OA) to synthesize $CsPbBr_3$ QDs which exhibited improved stability and PLQY.[32] Zhu et al. introduced thiocyanate (SCN^-) to synthesize NCs with increased PLQY almost by 10% and improved stability against air and moisture over several days due to the better passivation of trap states.[33] However, the ligand modification and elemental doping cannot improve the heat and humidity stability of QDs effectively. Among these methods, the coating technique is an effective method to enhance the optical performance and stability of NCs, which is due to their transparent characteristic, low cost, and the stability of coating components. Polymers,[34–40] metal-organic frameworks[41,42] and inorganic shells[43–46] have been reported to improve the optical performance and stability of NCs. However, the coating techniques for NCs are found to lead to the uncontrolled morphologies and sizes.[24,47–49] Specifically, inorganic shells with proper valence bands (VB) and conduction bands (CB) have been reported to play a crucial role in improving the luminescence and stability of NCs.[8] For tuning the charge or energy transfer process, the VB and CB of semiconductor are lower and higher than the NCs, respectively, that usually favors the carrier confine in the component with a narrower bandgap, leading to an

Q. Mo, W. Cai, S. Zhao, D. Yan, Z. Zang
Key Laboratory of Optoelectronic Technology & Systems
(Ministry of Education)
Chongqing University
Chongqing 400044, China
E-mail: zangzg@cqu.edu.cn

C. Chen
School of Microelectronics and Communication Engineering
Chongqing University
Chongqing 400044, China

The ORCID identification number(s) for the author(s) of this article can be found under https://doi.org/10.1002/lpor.202100278

DOI: 10.1002/lpor.202100278

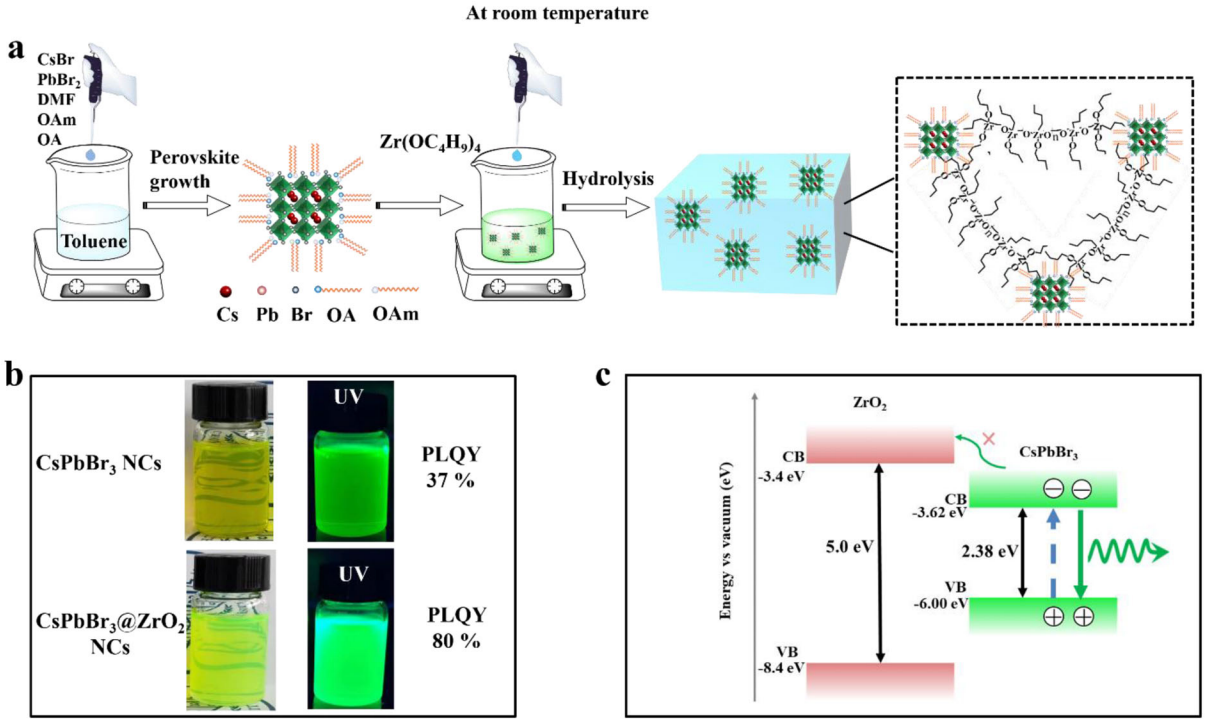

Figure 1. a) A schematic diagram of the reaction process of $CsPbBr_3@ZrO_2$ NCs. b) Images of $CsPbBr_3$ NCs and $CsPbBr_3@ZrO_2$ NCs without/with UV light of 365 nm. c) The scheme of the band structure and energy transfer of $CsPbBr_3/ZrO_2$ NCs.

enhanced radiative recombination.[50] To date, there are few reports about this structure. Carroll et al. reported that embedded nanocrystals of $CsPbBr_3$ in Cs_4PbBr_6 with enhanced PLQY.[51] Li et al. synthesized $CsPbBr_3/Rb_4PbBr_6$ core/shell nanocrystals with enhanced photostability by the shell coating of Rb_4PbBr_6.[52] Most recently, Zhang et al. prepared $CsPbBr_3/CsPb_2Br_5$ perovskite heterojunctions through a phase transition, the PLQY and stability enhanced owing to the heterojunction.[53] The above-mentioned methods most generally require high temperature, extra inert gases, and prolonged stirring,[8,33,40,48,49] which are complicated and time-consuming. Thus, it is urgent to develop a novel and room-temperature strategy to result in the uniform morphologies and sizes of NCs, the enhancement of optical performance and stability as well.

Herein, we present a facile method to prepare $CsPbBr_3@ZrO_2$ NCs at room temperature in air, and the whole process takes only 20 s. The obtained $CsPbBr_3$ NCs are embedded inside the ZrO_2 layer and uniformly dispersed without aggregation. A PLQY as high as 80% is achieved in the optimized $CsPbBr_3@ZrO_2$ NCs, while only 37% for the pure $CsPbBr_3$ NCs. Moreover, $CsPbBr_3@ZrO_2$ NCs exhibit excellent heat and moisture stability. Efficient WLEDs are also realized by combining blue InGaN chips with the prepared $CsPbBr_3@ZrO_2$ NCs and commercial $CaAlSiN_3:Eu^{2+}$ phosphors, which show excellent luminous efficacy of 64.0 Lm W^{-1}, correlated color temperature (CCT) of 4743 K and color coordinate of (0.351, 0.346). In addition, the high-performance WLEDs are used as visible light communication (VLC) sources with a -3 dB bandwidth of 2.75 MHz. Furthermore, on the basis of the white light system, a high data rate of 33.5 Mbps is achieved using orthogonal frequency division multiplexing (OFDM) modulation with bit loading, indicating their promising potential for high-speed communication. Therefore, we believe that $CsPbBr_3@ZrO_2$ NCs have great potential for both WLEDs and VLC communication based on their excellent optical properties and stability.

2. Results and Discussion

The $CsPbBr_3@ZrO_2$ NCs were obtained via a modified supersaturated recrystallization method at room temperature. CsBr and $PbBr_2$, as selected ion sources, were dissolved in N, N-dimethylformamide (DMF). Oleic acid (OA) and oleylamine (OAm) were then added as surface ligands, followed by a rapid injection into toluene. Upon the injection into the antisolvent of toluene, $CsPbBr_3$ NCs were formed immediately, as shown in **Figure 1**a. Then $Zr(OC_4H_9)_4$ was injected into the prepared $CsPbBr_3$ NCs solution to form ZrO_2 coating onto the NCs surface. The whole synthesis process was carried out at room temperature in air without extra inert gas and incorporation of water.

1) The hydrolysis reaction of the precursor with water in the air is suggested as follows:

$$Zr(OC_4H_9)_4 + 2H_2O \rightarrow Zr(OH)_2(OC_4H_9)_2 + 2C_4H_9OH \quad (1)$$

2) At the same time, the condensation reaction of the precursor is as follows:

$$Zr\text{-}OH + OH\text{-}Zr \rightarrow \text{-}Zr\text{-}O\text{-}Zr\text{-} + H_2O \quad (2)$$

$$Zr\text{-}OC_4H_9 + HO\text{-}Zr \rightarrow \text{-}Zr\text{-}O\text{-}Zr\text{-} + C_4H_9OH \quad (3)$$

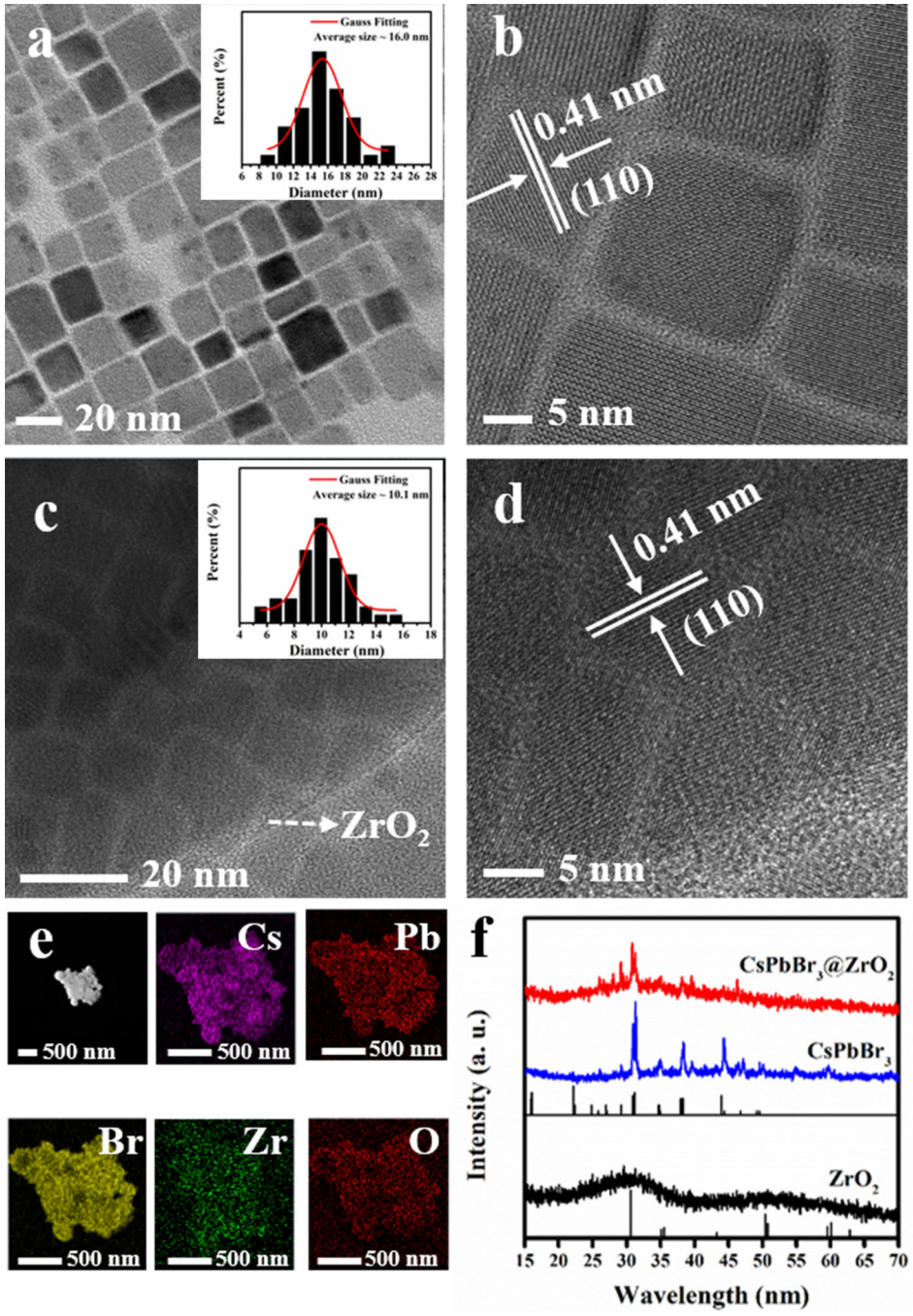

Figure 2. a,c) TEM images and b,d) HRTEM images of pure $CsPbBr_3$ and $CsPbBr_3@ZrO_2$ NCs. e) The element distribution of $CsPbBr_3@ZrO_2$ NCs. f) XRD patterns of ZrO_2, $CsPbBr_3$, and $CsPbBr_3@ZrO_2$ NCs.

In Figure 1b, the images of both $CsPbBr_3$ NCs and $CsPbBr_3@ZrO_2$ NCs exhibit green emission color, demonstrating its good color uniformity in normal and UV irradiation conditions. The luminescence of $CsPbBr_3@ZrO_2$ NCs is greener and PLQY is 80% which is higher than that $CsPbBr_3$ NCs of 37%. The scheme of the band structure in the $CsPbBr_3@ZrO_2$ NCs samples for explaining enhanced photoluminescence as compared to $CsPbBr_3$ NCs is shown in Figure 1c, the VB maximum position of $CsPbBr_3$ and ZrO_2 are estimated to be -6.00 and -8.4 eV,[52] respectively, and the conduction band (CB) minimum position are determined to be -3.62 and -3.4 eV,[52] respectively, with respect to the vacuum level. These results demonstrate the excitation and recombination processes associated with excitons of $CsPbBr_3@ZrO_2$ NCs, where the excitons were confined in the $CsPbBr_3$ NCs. Therefore, the radiative recombination may be enhanced to increase the emission efficiency of $CsPbBr_3$ NCs.

Figure 2a–d shows the transmission electron microscopy (TEM) and high-resolution TEM (HRTEM) images of $CsPbBr_3$

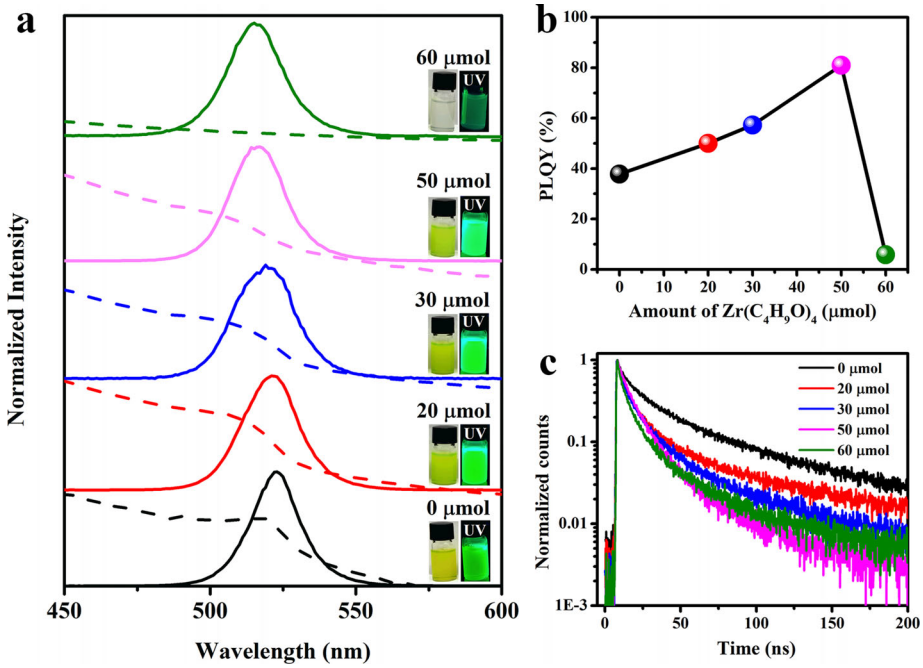

Figure 3. a) PL spectra (solid-line) and absorption spectra (dashed-line) (Insets show photographs of $CsPbBr_3@ZrO_2$ NCs solutions with/without UV light). b) PLQY and c) PL decay curves of $CsPbBr_3@ZrO_2$ NCs with different amount of $Zr(C_4H_9O)_4$.

and $CsPbBr_3@ZrO_2$ NCs, respectively. For $CsPbBr_3@ZrO_2$ NCs, as shown in Figure 2c,d, it is clear that an abundance of NCs is dispersed and embedded inside in the ZrO_2 shell. The corresponding HRTEM image of a typical single $CsPbBr_3@ZrO_2$ NCs suggests a lattice plane distance of 0.41 nm, which is consistent with the (110) plane of $CsPbBr_3$ NCs. In addition, compared with an average size of 16.0 nm for $CsPbBr_3$ NCs (Figure 2a), $CsPbBr_3@ZrO_2$ NCs exhibit a narrow size distribution with an average NCs size of 10.1 nm (Figure 2c). This phenomenon may be attributed to the etching of $CsPbBr_3$ NCs induced by n-butanol of zirconium n-butanol ($Zr(OC_4H_9)_4$), which results in size reduction. The distribution of Cs, Pb, Br, Zr, and O elements are clearly shown in the elemental mapping of the $CsPbBr_3@ZrO_2$ NCs (Figure 2e), indicating the presence of ZrO_2 in the NCs. The crystal structures of ZrO_2, $CsPbBr_3$, and $CsPbBr_3@ZrO_2$ NCs (50 μmol of $Zr(OC_4H_9)_4$) were then studied using X-ray diffraction (XRD) (Figure 2f). Two broad peaks located at 30.3° and 50.4° are clearly seen in prepared pure ZrO_2 powder using the same method, corresponding to the (011) and (112) planes of ZrO_2 (PDF#50-1089). The XRD results of $CsPbBr_3$ and $CsPbBr_3@ZrO_2$ NCs are indexed as the orthorhombic phase of $CsPbBr_3$ NCs (PDF#18-0364), and the existence of ZrO_2 could be observed in $CsPbBr_3@ZrO_2$ NCs. The X-ray photoelectron spectroscopy (XPS) of $CsPbBr_3@ZrO_2$ NCs was performed to clarify the existence of ZrO_2, as shown in Figure S1a (Supporting Information). Besides, the peaks of Cs 3d (738 and 724 eV, Figure S1b, Supporting Information), Pb 4f (143 and 138 eV, Figure S1c, Supporting Information), and Br 3d (68 eV, Figure S1d, Supporting Information) clearly demonstrate the formation of $CsPbBr_3$,[54] the peaks of Zr 3d (188 and 181 eV, Figure S1e, Supporting Information) and O 1s peak (532 eV, Figure S1f, Supporting Information) suggest the formation of ZrO_2 component.

Optical properties of $CsPbBr_3$ NCs and $CsPbBr_3@ZrO_2$ NCs were then studied, as shown in **Figure 3**a demonstrates the photoluminescence (PL) and absorption (Abs) spectrum of $CsPbBr_3@ZrO_2$ NCs with different amounts of $Zr(C_4H_9O)_4$. It is found that the increase of $Zr(C_4H_9O)_4$ leads to blue shifts of both PL emission peaks (from 523 to 515 nm) and Abs peaks (from 519 to 510 nm). The strong absorption in the short wavelength region confirms the ability of NCs to act as a color converter for blue LED chips. Moreover, with the increase of $Zr(C_4H_9O)_4$, the PLQY of $CsPbBr_3@ZrO_2$ NCs is found to be enhanced continually, as shown in Figure 3b. The PLQY of coating NCs reaches up to 80% with the addition of 50 μmol $Zr(C_4H_9O)_4$, which is higher than that of pure $CsPbBr_3$ NCs (37%). However, PLQY decreases with a further increase of $Zr(C_4H_9O)_4$, which might be due to the deterioration of $CsPbBr_3$ NCs induced from the large amount of $Zr(C_4H_9O)_4$ hydrolysis. Moreover, the time-resolved PL decay curves were studied (Figure 3c), in which average PL decay time (τ_{avg}) values of 33.2, 21.7, 17.4, 14.2, and 18.5 ns correspond to the NCs with the $Zr(C_4H_9O)_4$ of 0, 20, 30, 50, 60 μmol, respectively. With the increase of coating precursors, the reduction of transient lifetime values are may be resulted from the decrease of NCs sizes, which has been reported from previous works.[55,56] It was well known that the faster PL decay time could be caused by the smaller sizes due to stronger quantum confinement effects,[57,58] which is shown in Figure 2. To explore the origin of the enhanced PLQY, the radiative recombination rate (K_r) of these samples was estimated from the τ_{avg} and PLQY results according to the relevant equation,[59] and the detailed parameters are summarized in Table S1 (Supporting Information). When the molar of coating precursors increases from 20 to 60 μmol, the radiative recombination rate (K_r) is found to increase from 0.023 to 0.056 first, following by a significant reduction to

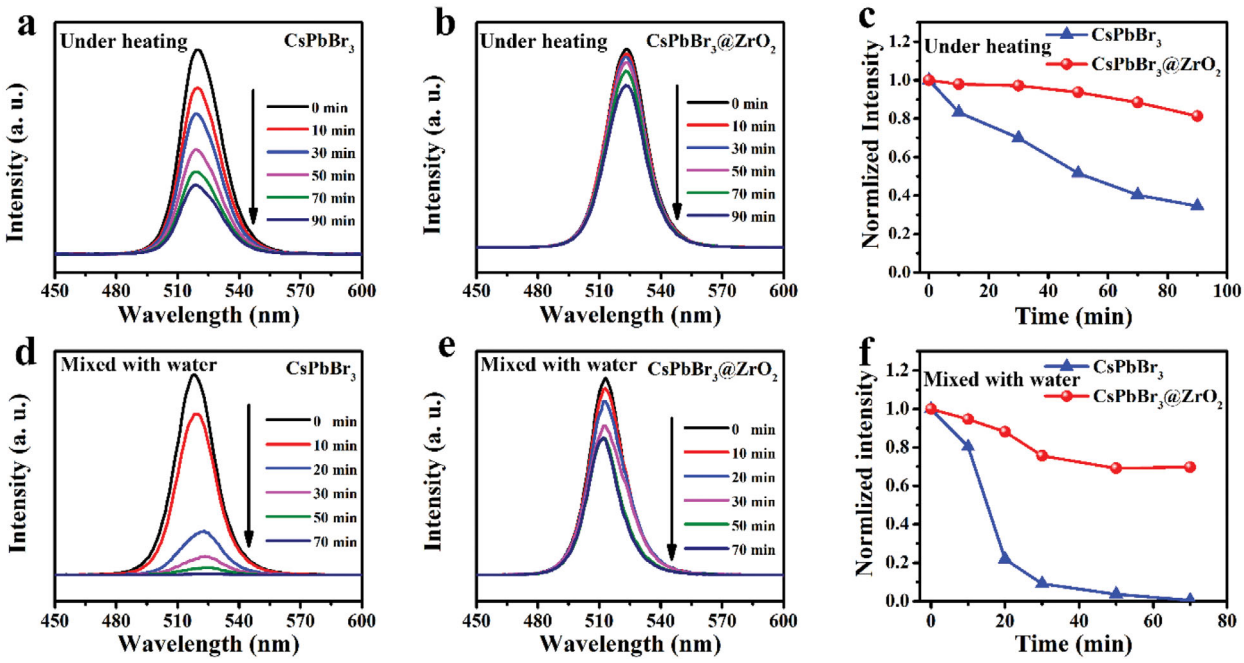

Figure 4. a,b) PL spectra and c) normalized PL intensity of $CsPbBr_3$ and $CsPbBr_3@ZrO_2$ under the heating of 60 °C. d,e) PL spectra and f) normalized PL intensity of $CsPbBr_3$ and $CsPbBr_3@ZrO_2$ in water.

0.003. It is in agreement with the changes of PLQY results, suggesting that the enhanced PLQY may be attributed to the enhancement of radiative recombination rate.

Subsequently, the heat and moisture effects on the PL performance of $CsPbBr_3$ and $CsPbBr_3@$ ZrO_2 NCs are tested, as shown in **Figure 4**. Compared with $CsPbBr_3$ NCs, $CsPbBr_3@$ ZrO_2 NCs film exhibits a relatively slow decrease in PL intensity upon the heating of 60 °C (Figure 4a,b). Although both films show a decrease of PL intensity over time, the $CsPbBr_3@$ ZrO_2 NCs film maintains 81% of its initial PL intensity after 90 min of continuous heating while only 34% remains in their counterparts, indicating that the $CsPbBr_3@$ ZrO_2 NCs film is fairly resistant to heat and possesses a good chemical stability (Figure 4c). Figure 4d,e shows the evolution of PL intensity for $CsPbBr_3$ and $CsPbBr_3@$ ZrO_2 NCs in equal amounts of water, respectively. After 70 min, the PL intensity of $CsPbBr_3$ quenches, while 70% of initial PL intensity maintains in $CsPbBr_3@$ ZrO_2 NCs. These results clearly imply that the coating with ZrO_2 can significantly enhance the heat and moisture stability of $CsPbBr_3$ NCs, which is critical for their practical applications in optoelectronics.

The excellent optical performance and stability of optimized $CsPbBr_3@$ ZrO_2 NCs can act as an important role in green emission, facilitating to application in the display. **Figure 5**a,b shows the electroluminescence (EL) spectra of WLEDs with $CsPbBr_3/CsPbBr_3@ZrO_2$ NCs and $CaAlSiN_3:Eu^{2+}$ at a driving voltage of 2.70 V, respectively. The CIE color coordinates of (0.342, 0.314), (0.351, 0.346) corresponding to $CsPbBr_3$ and $CsPbBr_3@ZrO_2$ WLEDs are shown in Figure 5c. Representative characteristics including CCT, luminous efficacy, and CIE coordinates of both WLEDs are summarized in **Table 1**. Notably, the luminous efficacy (64.0 Lm W^{-1}) of $CsPbBr_3@ZrO_2$ WLED is approximately 2.4 times to that of $CsPbBr_3$ WLED (26.9 Lm W^{-1}). The EL spectra of both $CsPbBr_3$ and $CsPbBr_3@ZrO_2$ WLEDs are then tested by varying driving voltage from 2.5 to 2.8 V. The color coordinates, CCT, and luminous efficacy of both WLEDs are found to change with the increase of driving voltages, as shown in Tables S2 and S3 (Supporting Information). The EL intensity of blue chip, NCs, and $CaAlSiN_3:Eu^{2+}$ increase with the increase of driving voltages. When the voltage is above 2.7 V, the EL intensity of green light for pure $CsPbBr_3$ NCs is lower than that of blue light, and the color coordinate changes from (0.347, 0.374) to (0.338, 0.280), indicating a poor stability of pure $CsPbBr_3$ NCs upon blue light excitation. In comparison, the $CsPbBr_3@ZrO_2$ NCs show an enhanced optical stability, in which the EL intensity of green light is higher than the blue light over the voltage range of 2.5 to 2.8 V and the color coordinate change from (0.353, 0.366) to (0.349, 0.343), as shown in Figure S2 (Supporting Information). The result suggests the excellent stability of the WLEDs with $CsPbBr_3@ZrO_2$ NCs under various driving voltages. To evaluate the performance of the fabricated WLEDs, the work is then compared with reported WLEDs of $CsPbBr_3$ NCs, as summarized in **Table 2** and Figure S3 (Supporting Information). Clearly, the performance of our WLEDs is better than most of the reported works, implying the promising potential of the WLEDs with $CsPbBr_3@ZrO_2$ NCs and $CaAlSiN_3:Eu^{2+}$ as the light source.

We further demonstrated the potential of the prepared WLEDs as a light source in a VLC system, as shown in **Figure 6**a. First, a bias T is adopted to combine the DC bias and the AC signal, and the output of the bias-T is used to modulate the blue chip. After that, the blue chip excites the $CsPbBr_3@ZrO_2$ NCs and the red phosphor to obtain white light for communication. Then, the optical signal is converted into an electrical signal by

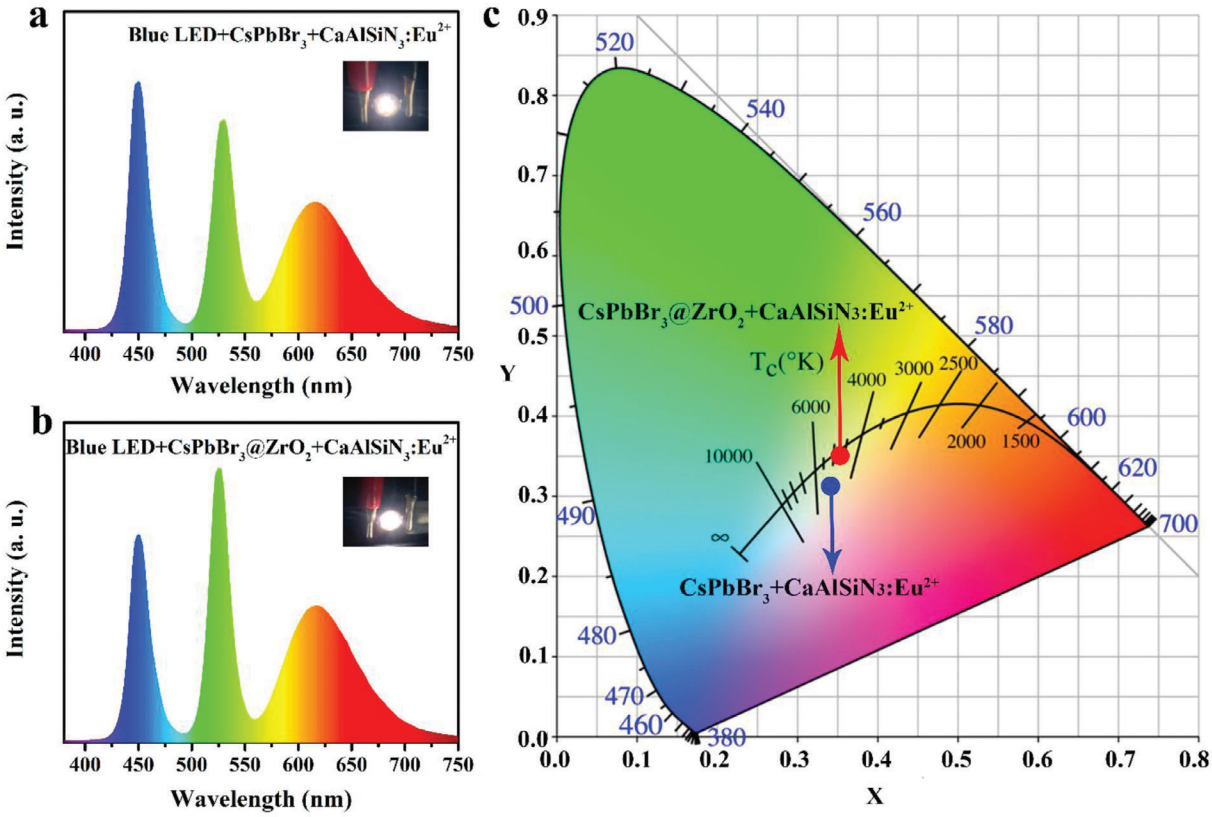

Figure 5. EL spectra of WLEDs based on a) $CsPbBr_3$ NCs or b) $CsPbBr_3@ZrO_2$ NCs and red phosphor $CaAlSiN_3:Eu^{2+}$. The insets show photographs of the WLEDs underworking. c) CIE chromaticity diagram of both WLEDs.

Table 1. Optical parameters of WLEDs.

Samples	CCT [K]	Luminous efficacy [Lm W^{-1}]	CIE coordinates [X, Y]
$CsPbBr_3$ & $CaAlSiN_3$: Eu^{2+}	4972	26.9	(0.342, 0.314)
$CsPbBr_3@ZrO_2$ & $CaAlSiN_3$: Eu^{2+}	4743	64.0	(0.351, 0.346)

using a photodetector (PD), which is further digitized through a digital storage oscilloscope (DSO). Figure 6b shows the measured electrical-optical-electrical (EOE)frequency response of the VLC system based on WLEDs at a DC bias voltage of 3 V, exhibiting a -3 dB bandwidth of about 2.7 MHz. In addition, Figure 6c shows the measured received signal-to-noise ratio (SNR) of the system with a modulation bandwidth of 10 MHz, where the SNR is gradually decreased with the increase of the frequency. By using OFDM modulation, adaptive bit loading according to the measured SNR performance can be applied to fully explore the achievable transmission data rate of the VLC system. The bit loading profile within the 10-MHz modulation bandwidth can be found in Figure 6d, where as high as 6 bits/s/Hz can be loaded to subcarriers within the low-frequency

Table 2. Comparisons with the $CsPbBr_3$ NCs based WLEDs reported previously.

Color converting materials	Synthesis method	CCT [K]	Luminous efficacy [Lm W^{-1}]	Refs.
$CsPbBr_3@SiO_2$ & $CsPb(Br/I)_3@SiO_2$ & $CsPbI_3@SiO_2$ composites	Antisolvent recrystallization method	5218	32.5	[3]
$CsPbBr_3@SiO_2$ & AgInZnS NCs	Anti-solvent recrystallization method	3689	40.6	[5]
$CsPbBr_3$/PMAO NCs & red nitride phosphor	Hot injection	3320	17.0	[36]
$CsPbBr_3$ NC & Mn-doped $CsPbBr_{0.5}I_{2.5}$ NCs	Hot injection	5498	29.7	[60]
$CsPbBr_3$ AeroPNCs &KSF phosphor	Hot injection	6500	59.8	[61]
$CsPbBr_3$ QD/silica & $CsPb(Br/I)_3$ QD/silica	Hot injection	NA	61.2	[48]
$CsPbBr_3$ NCs & $K_2SiF_6:Mn^{4+}$	Hot injection	4574	46.0	[62]
Red $CsPbBr_{1.5}I_{1.5}$-AlSt NCs & $YAG:Ce^{3+}$	Hot injection	4588	56.5	[63]
$CsPbBr_3@ZrO_2$ NCs & $CaAlSiN_3:Eu^{2+}$	Antisolvent recrystallization method	4743	64.0	This work

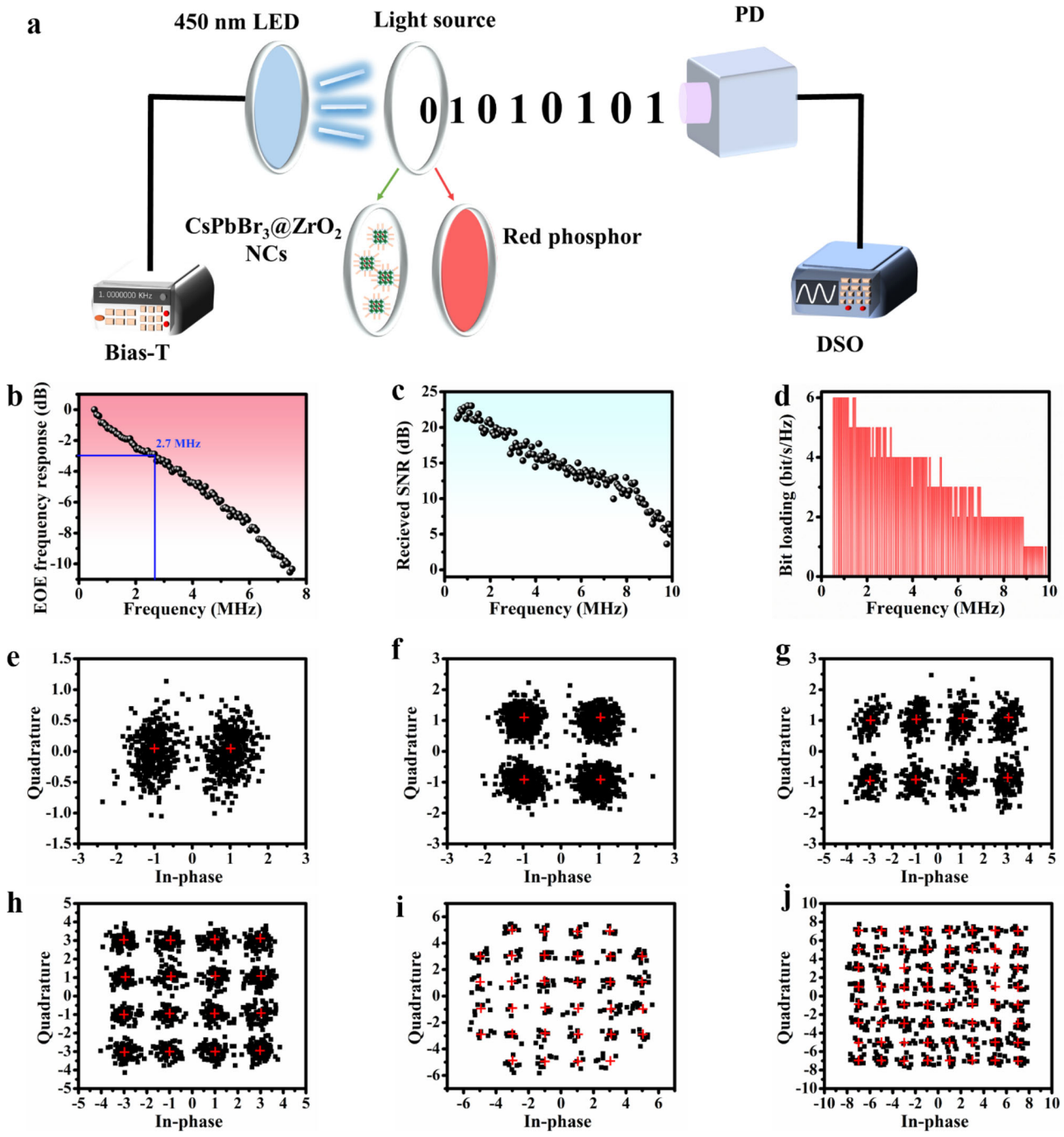

Figure 6. a) Schematic diagram of the experimental setup of the VLC system, b) EOE frequency response, c) received SNR, d) bit loading profile of the VLC system based on WLEDs, and e–j) the corresponding constellation diagrams of BPSK, 4QAM, 8QAM, 16QAM, 32QAM, and 64QAM, respectively.

region. Moreover, the corresponding received constellation diagrams of binary phase-shift keying (BPSK), 4-ary quadrature amplitude modulation (4QAM), 8QAM and 16QAM, 32QAM and 64QAM are shown in Figure 6e–j, respectively. By using the OFDM modulation with adaptive bit loading, the VLC system based on WLEDs shows a high transmission data rate up to 33.5 Mbps, which is more than 12 folds of the measured -3 dB bandwidth.

3. Conclusion

In summary, $CsPbBr_3@ZrO_2$ NCs were successfully synthesized by a facile method at room temperature in air. By optimizing the amount of $Zr(OC_4H_9)_4$, $CsPbBr_3@ZrO_2$ NCs exhibit high PLQY of 80% and excellent heat and moisture stability. Moreover, the efficient WLEDs were fabricated by combining the $CsPbBr_3@ZrO_2$ NCs with commercial red phosphor

$CaAlSiN_3:Eu^{2+}$, which exhibit an excellent luminescent performance, including color coordinate of (0.351, 0.346), correlated color temperature (CCT) of 4743 K, and luminous efficacy up to 64.0 Lm W^{-1}. In addition, the fabricated WLEDs are utilized for VLC, where a -3 dB bandwidth of 2.75 MHz and transmission data of 33.5 Mbps with OFDM modulation have been achieved. The results demonstrate that the simple method to coat $CsPbBr_3$ NCs with ZrO_2 at room temperature can enhance the optical efficiency and improve stability, and such an industry-compatible method may have potential applications in both solid-state lighting and optical wireless communication fields.

4. Experimental Section

Materials: $PbBr_2$ (99.99%) and CsBr (99.9%) were purchased from Xi'an Polymer Light Technology Corp. OA (90%), OAm (80-90%), DMF (99.9%), toluene (99.5%), and zirconium butoxide solution (80%) were purchased from Aladdin. All these chemicals were used without any further purification.

Synthesis of $CsPbBr_3$ NCs: $PbBr_2$ (0.4 mmol) and CsBr (0.4 mmol) were dissolved in 12 mL DMF. OAm (0.2 mL) and OA (0.6 mL) were added into the above precursor to act as the stabilizer. Then 0.5 mL of the precursor solution was quickly added into toluene (10 mL) under vigorous stirring at 1500 rpm for 10s.

Synthesis of $CsPbBr_3$@ZrO_2 NCs: Different amount of $Zr(OC_4H_9)_4$ (0, 20, 30, 50, 60 µmol) were injected into $CsPbBr_3$ NCs toluene solution (5 mL) and then vigorous vibrated for 10 s. After that, the mixture was centrifuged at 8500 rpm for 5 min to obtain the precipitates. Then the precipitates were re-dispersed and preserved in toluene. All the above experiments were carried out at room temperature in air.

Fabrication of White LED Devices: Polymethyl methacrylate (PMMA) solutions were first prepared by dissolving 15 mg PMMA in 1 mL toluene. Then the commercial red phosphor $CaAlSiN_3:Eu^{2+}$ and the PMMA mixed with $CsPbBr_3$ (or $CsPbBr_3$@ZrO_2) NCs were dropped on a blue chip.

Characterizations: XRD patterns were collected on a Cu Ka radiation (XRD-6100, SHIMADZU, Japan). XPS spectra were carried out on a ESCA Lab220I-XL. TEM measurements were performed on an electron microscope (Libra 200 FE, Zeiss, Germany). Absorption spectra were measured on a UV–vis spectrophotometer (UV–vis: UV-1800, SHIMADZU, Japan). Steady-state PL measurements were recorded by a fluorescence spectrophotometer (Agilent Cary Eclipse, Australia). PLQY and time-resolved fluorescence spectra were done on a spectrofluorometer (Edinburgh Instruments Ltd., FLS1000, United Kingdom). The optical parameters and electroluminescence spectra of the fabricated WLEDs were collected by a Keithley 2400 and a PR 670. The VLC system is illustrated in Figure 6a, a AC signal is generated by an arbitrary waveform generator (Rigol DG4102) and combined with a 3 V DC bias via a bias-T (Mini-Circuits Bias-Tee ZFBT-6GW+). Then the signal was employed to the WLEDs. After that, a photodetector (DH-GDT-D020V) with a -3dB bandwidth of 3 MHz was utilized, and the electrical signal was tested by a digital storage oscilloscope (LeCroy WaveSurfer 432). The output data were processed offline via MATLAB.

Supporting Information

Supporting Information is available from the Wiley Online Library or from the author.

Acknowledgements

This work was financially supported by the National Natural Science Foundation of China (11974063); Fundamental Research Funds for the Central Universities (2019CDJGFGD001).

Conflict of Interest

The authors declare no conflict of interest.

Data Availability Statement

Research data are not shared.

Keywords

$CsPbBr_3$ nanocrystals, stability, visible light communication, white light-emitting diodes, ZrO_2

Received: May 24, 2021
Revised: July 10, 2021
Published online:

[1] F. Zhang, Z. F. Shi, Z. Z. Ma, Y. Li, S. Li, D. Wu, T. T. Xu, X. J. Li, C. X. Shan, G. T. Du, *Nanoscale* **2018**, *10*, 20131.
[2] Y. Yue, D. Zhu, N. Zhang, G. Zhu, Z. Su, *ACS Appl. Mater. Interfaces* **2019**, *11*, 15898.
[3] H. Shao, X. Bai, G. Pan, H. Cui, J. Zhu, Y. Zhai, J. Liu, B. Dong, L. Xu, H. Song, *Nanotechnology* **2018**, *29*, 285706.
[4] T. Xuan, X. Yang, S. Lou, J. Huang, Y. Liu, J. Yu, H. Li, K. L. Wong, C. Wang, J. Wang, *Nanoscale* **2017**, *9*, 15286.
[5] H. Guan, S. Zhao, H. Wang, D. Yan, M. Wang, Z. Zang, *Nano Energy* **2020**, *67*, 104279.
[6] L. Qiu, H. Yang, Z. Dai, F. Sun, J. Hao, M. Guan, P. Dang, C. Yan, J. Lin, G. Li, *Inorg. Chem. Front.* **2020**, *7*, 2060.
[7] D. Yan, S. Zhao, H. Wang, Z. Zang, *Photonics Res.* **2020**, *8*, 1086.
[8] H. Liu, Y. Tan, M. Cao, H. Hu, L. Wu, X. Yu, L. Wang, B. Sun, Q. Zhang, *ACS Nano* **2019**, *13*, 5366.
[9] M. B. Faheem, B. Khan, C. Feng, M. U. Farooq, F. Raziq, Y. Xiao, Y. Li, *ACS Energy Lett.* **2019**, *5*, 290.
[10] J. Liang, D. Chen, X. Yao, K. Zhang, F. Qu, L. Qin, Y. Huang, J. Li, *Small* **2020**, *16*, 1903398.
[11] R. J. Sutton, G. E. Eperon, L. Miranda, E. S. Parrott, B. A. Kamino, J. B. Patel, M. T. Hörantner, M. B. Johnston, A. A. Haghighirad, D. T. Moore, H. J. Snaith, *Adv. Energy Mater.* **2016**, *6*, 1502458.
[12] Y. Wang, X. Li, J. Song, L. Xiao, H. Zeng, H. Sun, *Adv. Mater.* **2015**, *27*, 7101.
[13] C.-Y. Huang, C. Zou, C. Mao, K. L. Corp, Y.-C. Yao, Y.-J. Lee, C. W. Schlenker, A. K. Y. Jen, L. Y. Lin, *ACS Photonics* **2017**, *4*, 2281.
[14] H. Zhang, L. Yuan, Y. Chen, Y. Zhang, Y. Yu, X. Liang, W. Xiang, T. Wang, *Chem. Commun.* **2020**, *56*, 2583.
[15] P. Ramasamy, D. H. Lim, B. Kim, S. H. Lee, M. S. Lee, J. S. Lee, *Chem. Commun.* **2016**, *52*, 2067.
[16] C. Li, C. Han, Y. Zhang, Z. Zang, M. Wang, X. Tang, J. Du, *Sol. Energy Mater. Sol. Cells* **2017**,*172*, 341.
[17] T. Zhang, F. Wang, P. Zhang, Y. Wang, H. Chen, J. Li, J. Wu, L. Chen, Z. D. Chen, S. Li, *Nanoscale* **2019**, *11*, 2871.
[18] X. Li, Y. Wu, S. Zhang, B. Cai, Y. Gu, J. Song, H. Zeng, *Adv. Funct. Mater.* **2016**, *26*, 2435.
[19] Y. Wei, K. Li, Z. Cheng, M. Liu, H. Xiao, P. Dang, S. Liang, Z. Wu, H. Lian, *Adv. Mater.* **2019**, *31*, 1807592.
[20] E. V. Ushakova, A. I. Matuhina, A. V. Sokolova, S. A. Cherevkov, A. Dubavik, O. S. Medvedev, A. P. Litvin, D. A. Kurdyukov, V. G. Golubev, A. V. Baranov, *Nanotechnology* **2019**, *30*, 405206.
[21] J. Chen, K. Zidek, P. Chabera, D. Liu, P. Cheng, L. Nuuttila, M. J. Al-Marri, H. Lehtivuori, M. E. Messing, K. Han, K. Zheng, T. Pullerits, *J. Phys. Chem. Lett.* **2017**, *8*, 2316.
[22] X. He, C. Yu, M. Yu, J. Lin, Q. Li, Y. Fang, Z. Liu, Y. Xue, Y. Huang, C. Tang, *Inorg. Chem.* **2020**, *59*, 1234.

[23] S. Yuan, D. Chen, X. Li, J. Zhong, X. Xu, *ACS Appl. Mater. Interfaces* **2018**, *10*, 18918.
[24] Q. Zhong, M. Cao, H. Hu, D. Yang, M. Chen, P. Li, L. Wu, Q. Zhang, *ACS Nano* **2018**, *12*, 8579.
[25] Q. Mo, T. Shi, W. Cai, S. Zhao, D. Yan, J. Du, Z. Zang, *Photonics Res.* **2020**, *8*, 1605.
[26] S. Li, Z. Shi, F. Zhang, L. Wang, Z. Ma, D. Yang, Z. Yao, D. Wu, T.-T. Xu, Y. Tian, Y. Zhang, C. Shan, X. J. Li, *Chem. Mater.* **2019**, *31*, 3917.
[27] S. Huang, B. Wang, Q. Zhang, Z. Li, A. Shan, L. Li, *Adv. Opt. Mater.* **2018**, *6*, 1701106.
[28] J. H. Park, A. Y. Lee, J. C. Yu, Y. S. Nam, Y. Choi, J. Park, M. H. Song, *ACS Appl. Mater. Interfaces* **2019**, *11*, 8428.
[29] V. Naresh, N. Lee, *ACS Appl. Nano Mater.* **2020**, *3*, 7621.
[30] S. Thawarkar, P. J. S. Rana, R. Narayan, S. P. Singh, *Langmuir* **2019**, *35*, 17150.
[31] X. Liu, X. Zhang, L. Li, J. Xu, S. Yu, X. Gong, J. Zhang, H. Yin, *ACS Appl. Mater. Interfaces* **2019**, *11*, 40923.
[32] D. Yan, T. Shi, Z. Zang, T. Zhou, Z. Liu, Z. Zhang, J. Du, Y. Leng, X. Tang, *Small* **2019**, *15*, 1901173.
[33] S. Thapa, G. C. Adhikari, H. Zhu, P. Zhu, *J. Alloys Compd.* **2021**, *860*, 158501.
[34] J. Zhu, Z. Xie, X. Sun, S. Zhang, G. Pan, Y. Zhu, B. Dong, X. Bai, H. Zhang, H. Song, *Chem. Nano Mater.* **2018**, *5*, 346.
[35] Q. Zhou, Z. Bai, W. G. Lu, Y. Wang, B. Zou, H. Zhong, *Adv. Mater.* **2016**, *28*, 9163.
[36] H. Wu, S. Wang, F. Cao, J. Zhou, Q. Wu, H. Wang, X. Li, L. Yin, X. Yang, *Chem. Mater.* **2019**, *31*, 1936.
[37] A. Mikosch, S. Ciftci, G. Tainter, R. Shivanna, B. Haehnle, F. Deschler, A. J. C. Kuehne, *Chem. Mater.* **2019**, *31*, 2590.
[38] F. G. Weiqiang Yang, Y. Qiu, W. Z. Liu, H. Y. Xu, L. L. Yang, Y. C. Liu, *Adv. Opt. Mater* **2019**, *7*, 1900546.
[39] W. Yang, L. Fei, F. Gao, W. Liu, H. Xu, L. Yang, Y. Liu, *Chem. Eng. J.* **2020**, *387*, 124180.
[40] G. C. Adhikari, S. Thapa, H. Zhu, P. Zhu, *ACS Appl. Electron. Mater.* **2019**, *2*, 35.
[41] S. Jin, H. J. Son, O. K. Farha, G. P. Wiederrecht, J. T. Hupp, *J. Am. Chem. Soc.* **2013**, *135*, 955.
[42] L. Chen, R. Luque, Y. Li, *Chem. Soc. Rev.* **2017**, *46*, 4614.
[43] Z.-J. Li, E. Hofman, J. Li, A. H. Davis, C.-H. Tung, L.-Z. Wu, W. Zheng, *Adv. Funct. Mater.* **2018**, *28*, 1704288.
[44] Z. Li, L. Kong, S. Huang, L. Li, *Angew Chem., Int. Ed. Engl.* **2017**, *56*, 8134.
[45] H. C. Wang, S. Y. Lin, A. C. Tang, B. P. Singh, H. C. Tong, C. Y. Chen, Y. C. Lee, T. L. Tsai, R. S. Liu, *Angew. Chem., Int. Ed. Engl.* **2016**, *55*, 7924.
[46] F. Gao, W. Yang, X. Liu, Y. Li, W. Liu, H. Xu, Y. Liu, *Chem. Eng. J.* **2021**, *407*, 128001.
[47] X. Li, W. Cai, H. Guan, S. Zhao, S. Cao, C. Chen, M. Liu, Z. Zang, *Chem. Eng. J.* **2021**, *419*, 129551.
[48] C. Sun, Y. Zhang, C. Ruan, C. Yin, X. Wang, Y. Wang, W. W. Yu, *Adv. Mater.* **2016**, *28*, 10088.
[49] L. Qiu, J. Hao, Y. Feng, X. Qu, G. Li, Y. Wei, G. Xing, H. Wang, C. Yan, J. Lin, *J. Mater. Chem. C* **2019**, *7*, 4038.
[50] C. Jia, H. Li, X. Meng, H. Li, *Chem. Commun.* **2018**, *54*, 6300.
[51] J. Xu, W. Huang, P. Li, D. R. Onken, C. Dun, Y. Guo, K. B. Ucer, C. Lu, H. Wang, S. M. Geyer, R. T. Williams, D. L. Carroll, *Adv. Mater.* **2017**, *29*, 1703703.
[52] B. Wang, C. Zhang, S. Huang, Z. Li, L. Kong, L. Jin, J. Wang, K. Wu, L. Li, *ACS Appl. Mater. Interfaces* **2018**, *10*, 23303.
[53] Z. P. Huang, B. Ma, H. Wang, N. Li, R. T. Liu, Z. Q. Zhang, X. D. Zhang, J. H. Zhao, P. Z. Zheng, Q. Wang, H. L. Zhang, *J. Phys. Chem. Lett.* **2020**, *11*, 6007.
[54] S. Fang, G. Li, H. Li, Y. Lu, L. Li, *Chem. Commun.* **2018**, *54*, 3863.
[55] V. Malgras, S. Tominaka, J. W. Ryan, J. Henzie, T. Takei, K. Ohara, Y. Yamauchi, *J. Am. Chem. Soc.* **2016**, *138*, 13874.
[56] J. Feldmann, G. Peter, E. O. Gobel, P. Dawson, K. Moore, C. Foxon, R. J. Elliott, *Phys. Rev. Lett.* **1987**, *59*, 2337.
[57] X. Luo, R. Lai, Y. Li, Y. Han, G. Liang, X. Liu, T. Ding, J. Wang, K. Wu, *J. Am. Chem. Soc.* **2019**, *141*, 4186.
[58] H. Qian, Y. Xiao, Z. Liu, *Nat. Commun.* **2016**, *7*, 13153.
[59] N. Mondal, A. De, A. Samanta, *ACS Energy Lett.* **2018**, *4*, 32.
[60] M. He, S. Liu, L. Ding, Z. Zhang, J. Liu, W. Xiang, X. Liang, *J. Am. Ceram. Soc.* **2019**, *102*, 930.
[61] Z. Li, C. Song, J. Li, G. Liang, L. Rao, S. Yu, X. Ding, Y. Tang, B. Yu, J. Ou, U. Lemmer, G. Gomard, *Adv. Mater. Technol.* **2020**, *5*, 190094.
[62] H. Xu, J. Wang, T. Xuan, C. Lv, J. Hou, L. Zhang, Y. Dong, J. Shi, *Chem. Eng. J.* **2019**, *364*, 20.
[63] Y. Chang, Y. J. Yoon, G. Li, E. Xu, S. Yu, C. H. Lu, Z. Wang, Y. He, C. H. Lin, B. K. Wagner, V. V. Tsukruk, Z. Kang, N. Thadhani, Y. Jiang, Z. Lin, *ACS Appl. Mater. Interfaces* **2018**, *10*, 37267.